Energy & Buildings 268 (2022) 112236

Contents lists available at ScienceDirect

Energy & Buildings

journal homepage: www.elsevier.com/locate/enb

Development and optimization of highly efficient heat recoveries for low carbon residential buildings

Peng Liu [a,*], Maria Justo Alonso [a,b], Hans Martin Mathisen [b], Anneli Halfvardsson [c]

[a] SINTEF Community, Trondheim, Norway
[b] Department of Energy and Process Engineering, Norwegian University of Science and Technology, Trondheim, Norway
[c] Department of Research & Technology, Flexit AS, Ørje, Norway

ARTICLE INFO

Article history:
Received 26 October 2020
Revised 19 May 2022
Accepted 1 June 2022
Available online 4 June 2022

Keywords:
Energy efficient ventilation
Heat recovery
Heat wheel
Low-carbon buildings

ABSTRACT

To achieve energy efficiency and lower carbon emissions, building envelopes have become tighter and more insulated. These buildings must have mechanical ventilation with high efficient heat recovery to provide adequate indoor air quality using low energy in cold climates, and requirements for heat recovery efficiency are expected to increase. Today's aluminum heat wheels, one of the most commonly used heat recovery systems, may not be capable of providing such a high efficiency due to the presence of longitudinal heat conduction. This study focuses on developing highly efficient heat wheels by reducing the longitudinal heat conduction and enhancing heat transfer in different channel shapes and matrix materials for heat wheels. Previously often neglected, but in large heat wheels, the longitudinal heat conduction can result in a significant efficiency reduction effect. The highly efficient heat wheels are sought via parametric analysis, experimental verification, and optimization in this study. Reducing matrix wall thickness for high conductive materials and using low conductive materials can significantly improve temperature efficiency. The calculated and experimental results show that the developed plastic and stainless steel heat wheels can exhibit high temperature efficiency of over 90% with acceptable pressure drops. However, stainless steel's high cost and stiffness may limit its use in heat wheels. Wheels made of plastic with circular channels that are symmetrical could be a promising solution to meet the high temperature efficiency needs of the future. Additionally, the optimization shows that the temperature efficiency of plastic heat wheels is more sensitive to design parameters than aluminum or stainless-steel wheels.

1. Introduction

Buildings account for around 40 % of global energy use: 40 % in the EU[1], 30 % in China [2], 41 % in the US [3] and 39 % in the UK [4]. This has surpassed the other major sectors, e.g., industrial and transportation [5]. Energy consumption in buildings is forecasted to grow by 34 % over the next 20 years [6]. Heating, ventilation, and air-conditioning (HVAC) systems consume 40 %-60 % of the energy in buildings without heat recovery [5]. Using high insulation and airtight envelopes are energy-efficient measures commonly utilized to reduce the heat loss caused by the transmission and infiltration losses in cold climates. In such envelopes, heating the ventilation air to ensure the desired supply air temperature is energy intensive. Heat recovery reduces energy demands for heating ventilation air whilst maintaining sufficient ventilation rates. In cold climates, various types of heat recovery systems have been extensively applied and studied for residential buildings [7–11].

The use of heat recovery and its minimum temperature efficiency is required in many countries building codes [11]. As an example, the yearly average temperature efficiency is required to be at least 80 % in Norwegian residential buildings [12]. Nevertheless, to the authors' knowledge, this efficiency is rarely achieved in practice. The operational heat recovery efficiency varies with wheel design, airflow rates, supply air temperature setpoint, leakage levels and operating conditions such as condensation and frost [13–15]. All these factors may, in practice, hinder the operational recovery efficiency, although the designed temperature efficiency could be very high.

The working principle of a heat wheel is illustrated in Fig. 1. The heat in the extract air is stored in the matrix in contact with it. The matrix is the metallic heat transfer surface in a heat wheel. The stored heat in the matrix is then released into the supply air through heat convection. The cold outdoor air is heated by the recovered heat from the extract air that would otherwise be lost.

* Corresponding author.
E-mail address: peng.liu@sintef.no (P. Liu).

https://doi.org/10.1016/j.enbuild.2022.112236
0378-7788/

Nomenclature

Parameters

	Heat transfer area [m^2]
A_k	Cross-sectional area of the matrix wall [m^2]
B	Bias uncertainty
C^*	Ratio of minimum to maximum heat capacity rates
C_{min}	Minimum heat capacity rate [W/K]
C_r^*	Ratio of total matrix heat capacity rate
G	Fluid mass velocity based on the minimum free area [kg/m^2]
g_c	Proportionality constant
h	Convective heat transfer coefficient [W/m^2 K]
k	Thermal conductivity [W/(mK)]
L	Depth of the wheel [m]
m	Mass flow rate [kg/s]
N	Rotation speed [RPM]
P	Precision uncertainty
Re	Reynolds number [m^2]
U	Overall heat transfer coefficient [W/m^2 K]
U_r	Total uncertainty
X	Measured variable

Abbreviations

AL	Aluminum
CIR	Circular
LHC	Longitudinal heat conduction
NTU	Number of transfer units
PL	Plastic
REC	Rectangular
SIN	Sinusoidal
SS	Stainless steel

Greek letters

α	Aspect ratio of the channel
λ	Dimensionless indicator of longitudinal heat conduction
δ	Thickness of the wall [m]
Δp	Pressure drop [Pa]
ε	Temperature efficiency
$\Delta\varepsilon$	Inefficiency

With heat transfer occurring in a heat exchanger, temperature gradients exist in both airflows and in the rotary matrix. The resulting heat conduction from the high to the low temperature ends in air and the wheel matrix influences the heat transfer rates between the airflows. The heat conduction in the air is usually negligible [16]. In contrast, the longitudinal heat conduction (LHC) in the metallic matrix is illustrated in Fig. 1. LHC acts as a dissipation source, which may significantly lower the temperature difference between two ends of the matrix and dramatically reduce the temperature efficiency [16].

A heat wheel with the counterflow airflow arrangement has theoretically a relatively high efficiency. However, field measurements of heat wheels in buildings have shown that the actual efficiency can be dramatically lower than designed or predicted [17,18]. There are different reasons for the unexpectedly low efficiency: 1) longitudinal heat conduction along with the metallic matrix in the airflow direction, as shown in Fig. 1; 2) leakages caused by the rotation and improper installation [18–20] and 3) the formation and accumulation of ice and frost inside the heat wheel [21,22]. To the best of the authors' knowledge, the LHC effect has been often overlooked in the study of heat wheel efficiency although this effect is significant particularly for the designed high temperature efficiency. As an example, an aluminum heat wheel may have a temperature efficiency of 70% when it is designed to be 90 without considering the LHC effect [16]. Consequently, one may over-predict the energy savings from the heat recovery and under-size the supply air heating coils which may result in thermal discomfort, e.g., a draught due to low supply air temperatures. Ignoring the heat wheel's LHC effect causes incorrect predictions of energy use and thermal discomfort. Liu et al. [17] found that the efficiency discrepancy between the field measurement and predicted efficiency in the heat wheel is mainly caused by the effect of the LHC for a renovated zero emission office building in Norway. The heat transfer in a heat wheel with longitudinal heat conduction has been modelled and solved both analytically and numerically [23–25]. Correlations developed on the basis of analytical and numerical solutions are available for predicting the temperature efficiency with LHC [16,24].

Corrugation shapes and geometries of the wheel matrix determine the compactness of the heat wheel, which is related to the total heat transfer area and overall heat transfer coefficient. Certain corrugations, such as sinusoidal and rectangular shapes, lead to stagnant zones owing to their asymmetrical resistance to the flow [26]. Matrix materials with high thermal conductivity compensate for stagnant zones by conducting heat peripherally around the channel walls. Nevertheless, for the less conductive materials, peripheral heat conduction is less efficient near stagnant zones, thus the heat capacity is underutilized [27]. When symmetric shapes are used, such as a circle, stagnant zones are minimized, and all materials have the same convective heat transfer. Low thermal conductivity reduces longitudinal heat conduction, but it can also negatively impact the thermal boundary conditions for heat convection [27]. Thus, the matrix corrugation shape and its geometry, together with the material's conductivity are essential factors to optimize when designing highly efficient heat wheels as they affect heat transfer coefficients and heat transfer areas.

Smith and Svendsen [27] developed a plastic heat wheel for room-based ventilation in temperate climates. The plastic heat wheel is able to exceed 80 % for a balanced ventilation rate of 28 m^3/h, but its performance for a higher ventilation rate, e.g. a single family (in a range of 150 m^3/h to 500 m^3/h), is not reported. Borodulin and Nizovtsev [28] constructed a mathematical model of the regenerative heat exchanger with periodic changes of airflow direction. The analysis indicates that longitudinal heat flux in the matrix must be taken into account, which is critical for materials with high thermal diffusivity. The efficiency decreases as the thermal diffusivity of the matrix material increases. The replacement of polypropylene with aluminum therefore results in a 20% decrease in effectiveness. The corrugation shapes and geometries are not investigated in their study. In another study [29], a theoretical model to predict the heat and mass transfer performance of a plastic rotary regenerator considering leakage and adsorption were developed. The design parameters of a plastic rotary regenerator were optimized to improve the cooling and dehumidifying performance of a desiccant air-conditioning system. The optimum temperature efficiency of 85% was identified.

Even though the performance and influencing design parameters of heat wheels have been extensively investigated, studies accessing the combined heat transfer characteristics from matrix materials, matrix corrugation shapes and geometries are very lim-

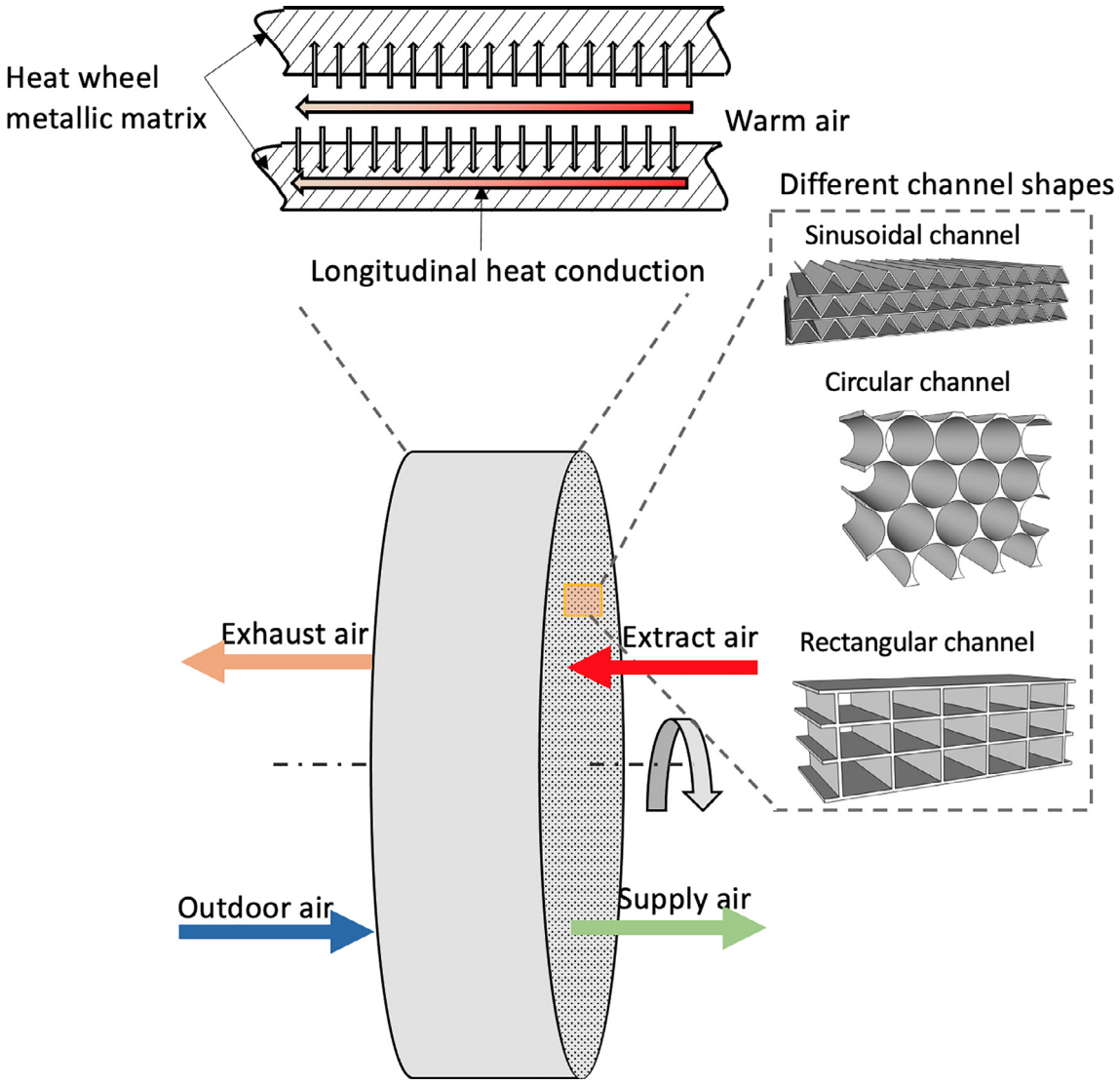

Fig. 1. Schematic view of a heat wheel and longitudinal heat conduction for different channel shapes.

ited. Heat recovery efficiency requirements may increase for residential buildings to achieve zero emissions. However, to the authors' knowledge, there is a lack of feasible heat wheels with extraordinarily high efficiency (e.g., >90%) for residential ventilation systems. This study is focused on developing solutions to reduce the effect of LHC and significantly improve the temperature efficiency of heat wheels with parametric analysis and optimal design. The heat wheels with different materials including aluminum, stainless steel and plastic and different channel shapes including sinusoidal, circular and rectangular channels are investigated. The prototypes of heat wheels with high temperature efficiency are developed and experimentally tested to validate the theoretical development. Parametric study and optimization are performed to investigate the effects of various input parameters and maximize the temperature efficiency.

2. Methods

This chapter presents the theoretical models for temperature efficiency and pressure drop through the exchanger core. The calculated temperature efficiency and pressure drop were validated by experimental data. The experimental measurements and uncertainty analysis were presented at the end of this section.

2.1. Modelling temperature efficiency of heat wheel: $\varepsilon - NTU$ method

The correlation for efficiency developed by Kays and London [30] is given below. The LHC effect on thermal efficiency was not included in this correlation.

$$\varepsilon_{exclude\_LHC} = \frac{NTU_o}{1+NTU_o}\left(1-\frac{1}{9C_r^{*1.93}}\right) \quad (1)$$

Where NTU_o is the number of the heat transfer unit and.$NTU_o = U_0A/(\dot{m}Cp)_{min}$

C_r^* is the ratio of total matrix heat capacity rate, which is C_r/C_{min}.

Shah [24] developed a correlation considering the LHC to determine the recovery efficiency of the heat wheel ($\varepsilon_{include\_LHC}$) based on numerical solutions from [23]. Our research aims to improving the temperature efficiency of heat wheels including LHC effect (namely $\varepsilon_{include\_LHC}$). The correlation is given in Eq. (2).

$$\varepsilon_{include\_LHC} = \frac{NTU_o}{1+NTU_o}\left[1-\frac{1}{9(C_r^*)^{1.93}}\right]\left(1-\frac{C_\lambda}{2-C^*}\right) \quad (2)$$

C_λ in Eq. (2) can be calculated from,

$$C_\lambda = \frac{1}{1+NTU_o(1+\lambda\Phi)/(1+\lambda NTU_o)} - \frac{1}{1+NTU_o} \quad (3)$$

Table 1
Nusselt number for different channel shapes and different conductive materials in laminar flow.

Channel shape	Nu_{H1} for high conductive materials, Nu_{H2} for low conductive materials
SIN	$Nu_{H1} = 1.9030(1 + 0.4556\alpha + 1.2111\alpha^2 - 1.6805\alpha^3 + 0.7724\alpha^4 - 0.1228\alpha^5)$ For $0 \le \alpha \le 2$
	$Nu_{H2} = 0.76\alpha$ For $0 \le \alpha \le 0.125$
	$Nu_{H2} = -0.0202(1 - 32.0594\alpha - 216.1635\alpha^2 + 244.3812\alpha^3 - 82.4951\alpha^4 + 7.6733\alpha^5)$ For $0.125 \le \alpha \le 2$
CIR	Nu_{H1} =4.364
	Nu_{H2} =4.364
REC	$Nu_{H1} = 8.235(1 - 2.0421\alpha + 3.0853\alpha^2 - 2.4765\alpha^3 + 1.0578\alpha^4 - 0.1861\alpha^5)$ For $0 \le \alpha \le 1$
	$Nu_{H2} = 8.235(1 - 10.6044\alpha + 61.1755\alpha^2 - 155.1803\alpha^3 + 176.9203\alpha^4 - 72.9236\alpha^5)$ For $0 \le \alpha \le 1$

Table 2
Design and operating parameters for the studied heat wheels.

ID	Parameter	Value	ID	Parameter	Value
1	Wheel depth	200 mm	5	Ventilation rate	150 m^3/h - 500 m^3/h
2	Wheel diameter	500 mm	6	Air density	1.2 kg/m^3
3	Wall thickness	0.065 mm	7	Rotary speed	10 RPM
4	Wall material	AL: k =205 W/(m·K) c_p = 900 J/(kg·K)	8	Channel shape	SIN: Channel height: 1.6 mm Channel period: 3.5 mm
		SS: k =16 W/(m·K) c_p = 502 J/(kg·K)			CIR: Channel diameter: 2.0 mm
		PL: k =0.2 W/(m·K) c_p = 1200 J/(kg·K)			REC: Channel height: 2.0 mm Channel width: 4.0 mm

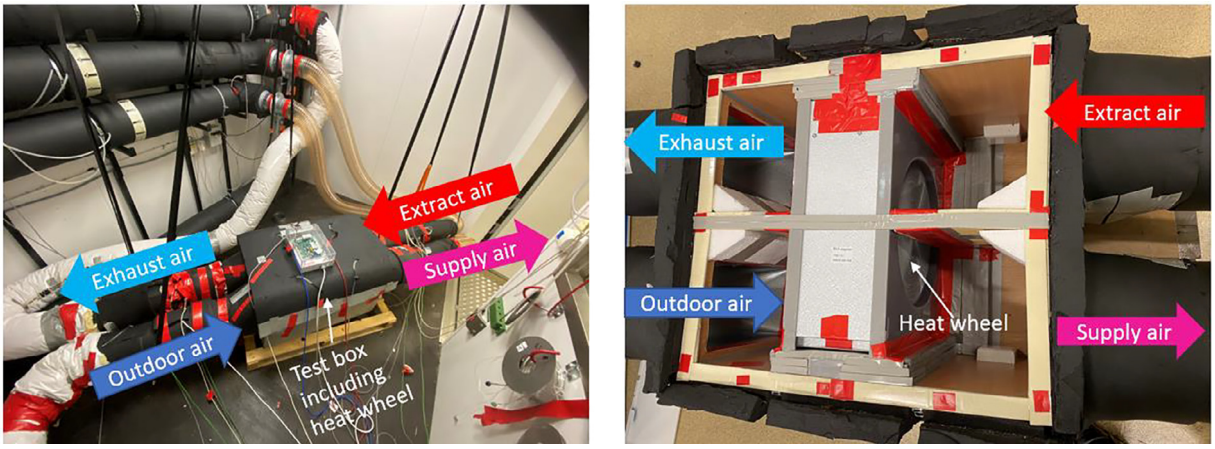

Fig. 2. Pictures of the testing box, connected airflows and tested heat wheel.

$$\Phi \approx \left(\frac{\lambda NTU_o}{1+\lambda NTU_o}\right)^{1/2} tanh\left\{\frac{NTU_O}{[\lambda NTU_o/(1+\lambda NTU_o)]^{1/2}}\right\} \quad (4)$$

According to the analysis in Ref [16], for NTU≥ 3,

$$\Phi \approx \left(\frac{\lambda NTU_o}{1+\lambda NTU_o}\right)^{1/2} \quad (5)$$

λ is a dimensionless parameter that refers to a ratio of longitudinal heat conduction along with flow direction per unit length to the heat capacity of the air per unit temperature difference. λ is given as the following equation.

$$\lambda = \frac{k_m A_k}{LC_{min}} \quad (6)$$

λ indicates the effect of LHC on heat recovery efficiency. The higher the value of λ, the higher the heat conduction loss in the heat wheel matrix and, therefore, the lower the exchanger temperature efficiency. Eq. (6) shows that the LHC effect is proportional to the thermal conductivity of the matrix material and the cross-sectional area of the matrix of the heat wheel and inversely proportional to the depth of the wheel and the heat capacity of the airflow. The inefficiency $\Delta\varepsilon$, which is referred to the efficiency reduction due to the presence of the LHC effect, can be estimated with Eq. (7) [16].

$$\frac{\Delta\varepsilon}{\varepsilon} = \frac{\varepsilon_{\lambda=0} - \varepsilon_{\lambda\neq 0}}{\varepsilon_{\lambda=0}} \quad (7)$$

According to Eq. (2) and Eq. (7), the efficiency reduction owing to the LHC effect is a function of NTU and λ. Increasing values of NTU and λ increase LHC's penalty to the temperature efficiency. Thereafter, the efficiency reduction is higher when high efficiency is sought. As an example, the ineffectiveness is>10% for all λ > 0.08 where NTU0 < 15 [30]. Thus, the LHC effect must be considered when designing highly efficient heat wheels.

NTU_o is the modified number of transfer units, which is.

$$NTU_o = \frac{U_o A}{(\dot{m}Cp)_{min}} \quad (8)$$

The overall heat transfer coefficient U_o is given by.

$$U_o = \left(\frac{2}{h} + \frac{\delta}{3k_m}\right)^{-1} \quad (9)$$

The transverse heat conduction resistance of the heat wheel matrix can be calculated by $\frac{\delta}{3k_m}$ based on Shah and Sekulic [16].

Therefore, the convective heat transfer coefficient for the warm and cold sides, h, is more crucial to determine and can be calculated by.

$$h = \frac{Nuk_{air}}{D_h} \tag{10}$$

Nusselt number, Nu, which refers to the ratio of convective to conductive heat transfer, is sensitive to the channel geometry and the thermal boundary conditions for the laminar flow regime. The airflow is assumed to be thermally fully developed due to the short thermal entrance length. The thermal boundary condition with a constant heat flux rate is applied for the counterflow heat wheels. The boundary conditions can be further divided as H1 and H2 conditions based on the conductive ability of the material [16]. The H1 condition can be realized for highly conductive materials such as aluminum, copper, and stainless steel, and H2 can be realized for poorly conductive materials such as plastic or ceramics. The Nusselt number for different channel geometries and thermal boundary conditions used in this study are listed in Table 1. Nu_{H1} represents highly conductive material and Nu_{H2} poorly conductive material. The aspect ratio α is the ratio of channel height to the width.

Using the method developed in this section, the temperature efficiency of an aluminum heat wheel with sinusoidal corrugation is calculated including and excluding the LHC effect. An aluminum heat wheel with the sinusoidal channel shape is used as the baseline case to assess the influence of LHC and NTU. Table 2 presents parameters for the studied heat wheels with three different conductive materials, including aluminum stainless steel or plastic, and different channel shapes, including sinusoidal, circular and rectangular channels.

2.2. Pressure drop through heat wheel core

The calculation of the pressure drop in a heat wheel is essential for determining fan power in ventilation. The airflow regime in this study is laminar with a Reynolds number much lower than 2300. The total core pressure drop consists of the pressure loss due to the entrance effect, the pressure rise due to the exit effect and the core friction pressure loss. The friction pressure loss is generally the dominant term, about 90 % or more of the pressure drop for gas flow. The pressure loss and the pressure rise caused by the entrance and exit usually compensate each other. The friction pressure loss through a heat wheel is approximated by the following equation [16]:

$$\Delta p \approx \frac{4fLG^2}{2g_c D_h} \tag{11}$$

The friction factor f experimentally derived [16], for the different channel shapes and aspect ratios in a laminar flow, is used in this study.

2.3. Experimental study and measurement uncertainties

The calculated temperature efficiency and pressure drop for different heat wheels are experimentally validated in a test rig built to satisfy EN308:1997 [31] requirements. The test rig and its connections to the different airflows are illustrated in Fig. 2. The test box is constructed so that different heat wheels can be replaced and tested at the same testing conditions. The temperature efficiency and pressure drop through the developed heat wheels were experimentally measured according to the standard EN308:1997 [31] under the dry testing condition. The dry bulb temperature of the outdoor air was 5 ℃, the extract air was 25 ℃, and the extract air relative humidity was lower than 30%. Air static pressure was measured at the air ducts in the direction of the airflow before and after the testing box. Airflow rates were measured according to ISO 5167–1:2003 and ISO5167-2:2003 [32,33] using orifice plates with corner tapings. Static pressure 0 Pa was maintained in the outdoor and exhaust air static pressure measurement points in the air ducts. Static pressure measurement points of the testing box were also recorded separately.

Four prototype heat wheel cores were constructed and tested in accordance with the testing standard EN 308 [31]. They are as follows: (1) AL SIN, an aluminum wheel with channel height of 1.4 mm, channel period of 3.0 mm, wheel diameter of 400 mm, wheel depth of 150 mm and matrix wall thickness of 0.08 mm; (2) SS SIN, a stainless steel wheel with the same geometry as the wheel (1); (3) CIR 2.5, a plastic wheel with a circular channel and diameter of 2.5 mm; (4) CIR 3.5, a plastic wheel with a circular channel and diameter of 3.5 mm.

The total uncertainty consists of the bias and the precision uncertainties [34]. The total uncertainty can be determined by Eq. (12).

$$U_r = \sqrt{\left[\left(\frac{\partial r}{\partial X_1}U_{X_1}\right)^2 + \left(\frac{\partial r}{\partial X_2}U_{X_2}\right)^2 + \cdots + \left(\frac{\partial r}{\partial X_i}U_{X_i}\right)^2\right]} \tag{12}$$

Where, U is the total uncertainty for the measured variables, and it can be calculated using Eq. (13).

$$U_{x_i} = \sqrt{B^2 + P^2} \tag{13}$$

The measurements have been conducted so that the uncertainty demands set in the standard EN 308:1997 are fulfilled. The total uncertainty of temperature measurements using Pt 100 sensor is ± 0.1 °C, and the total uncertainty of the airflow measurements using orifice plates and manometers is ± 1.5 %. The total uncertainty of the static pressure measurement is ± 1.0 % of the measured values. The estimated uncertainty of temperature efficiency is ± 3.0 % of the indicated values.

Table 3
Lower and upper bounds, and values of the parameters for efficiency optimization.

ID	Parameter	[Lower bound, upper bound] or fixed values	ID	Parameter	[Lower bound, upper bound] or fixed values
1	Wheel depth	[100, 200] mm	5	Airflow rate	200 m3/h
2	Wheel diameter	[200, 800] mm	6	Air density	1.2 kg/m3
3	Wall thickness	[0.06, 0.10] mm	7	Rotary speed	10 RPM
4	Wall material		8	Channel shape	
	AL	k =205 W/(m·K) c_p = 900 J/(kg·K)		SIN	Channel hetight: [1, 4] mm
	SS	k =16 W/(m·K) c_p = 502 J/(kg·K)			Channel period: [1, 4] mm
	PL	k =0.2 W/(m·K) c_p = 1200 J/(kg·K)		CIR	Channel diameter: [1, 4] mm
				REC	Channel height: [1, 4] mm
					Channel width: [1, 4] mm

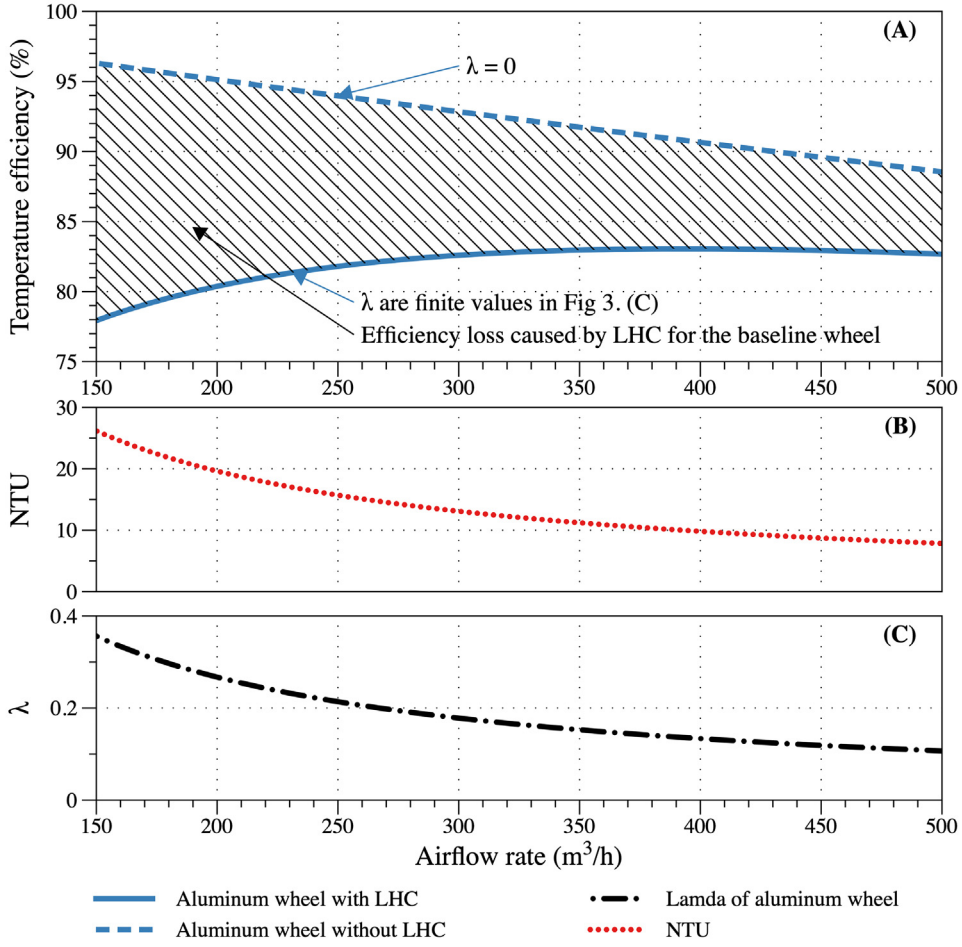

Fig. 3. (A) Temperature efficiency of the baseline aluminum wheel with and without LHC vs airflow rate, (B) NTU vs airflow rate, and (C) λ vs airflow rate.

2.4. Optimization of temperature efficiency of heat wheels

The Pattern Search optimization algorithm is applied to find the heat wheel designs that produce the maximum and minimum temperature efficiency in MATLAB. The optimization considering the influence of different design parameters shows the maximum potential efficiency of the different wheels. The pattern search optimization is performed in this study to demonstrate a feasible method to achieve optimal design. The optimal designs, however, cannot be experimentally validated because the optimal materials, corrugations, and geometries were not available for the construction of the heat wheels. The reader is referred for further explanations about the optimization method to [35]. The pattern search algorithm seeks a minimum function value. The maximum temperature efficiency can be found by making the objective function Eq. (2) negative. The pattern search algorithm is relatively robust and efficient for a small and medium search area and this method can be applied to objective functions that are not continuous or not differentiable. Therefore, the pattern search optimization method can be used for the nonlinear temperature efficiency model presented in Section 2.1 of this study. The flow rate is set at a constant of 200 m^3/h to represent the typical ventilation rate in a single family house. The lower and upper bounds used for optimizing the studied heat wheels are presented in Table 3.

The objective function for optimization is Eq. (2). The aspect ratio α, as the ratio of channel height to the channel width (period), is constrained to $0 < \alpha < 2$ for the sinusoidal channel and $0 < \alpha < 1$ for the rectangular channel. The lower and upper bounds and values of the parameters for efficiency optimization are given in Table 3. The criteria to stop the optimization are set with a tolerance of input parameters, function values and searching mesh size lower than 1e-6.

3. Results and discussion

The aluminum heat wheel with a sinusoidal channel shape is modelled with the methods mentioned earlier and sequentially used as a reference for parametric analysis. Thereafter, the influence of the wheel design and operating parameters on temperature efficiency is studied and compared. The predicted temperature efficiency and pressure drop for the wheels are validated against experimental results. Lastly, the heat wheels with different wall materials and channel shapes are theoretically optimized to achieve maximum temperature efficiency.

3.1. Performance of an aluminum heat wheel with a sinusoidal channel shape

Fig. 3 (A) shows the temperature efficiency for the baseline wheel against the ventilation rates ranging from 150 m^3/h to 500 m^3/h. This airflow rate range is the most frequently used for single family houses according to the Norwegian building requirement TEK17 [12], which is in line with the European standard EN

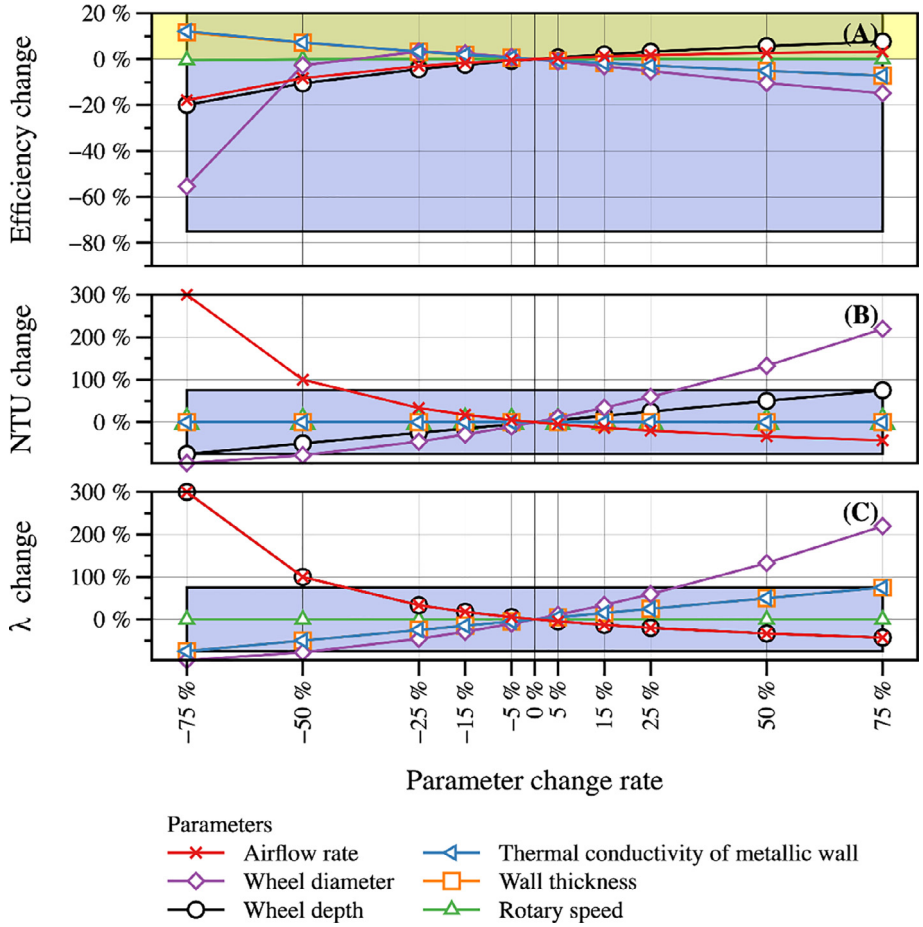

Fig. 4. Parametric analysis for (A) temperature efficiency, (B) NTU, and (C) λ.

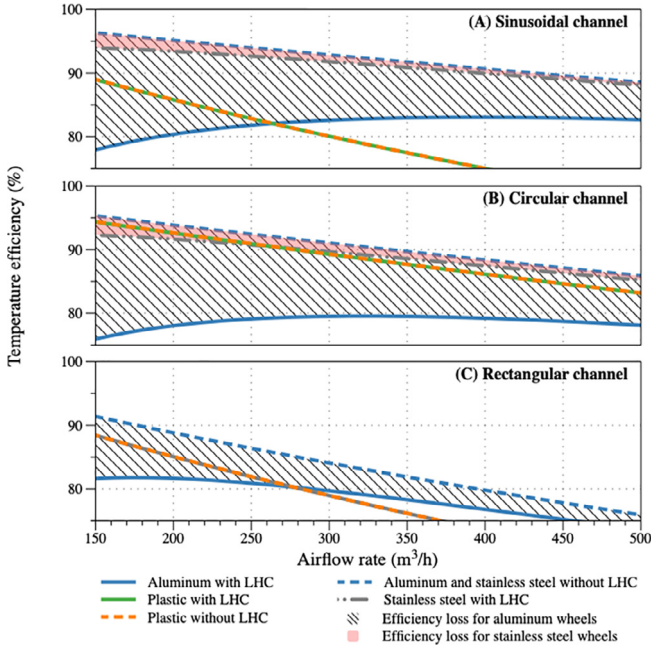

Fig. 5. Temperature efficiency of aluminum, stainless steel and plastic heat wheel vs airflow rates with (A) sinusoidal, (B) circular, and (C) rectangular channel shapes.

16,798 for category II air quality when low emission materials are used in the building.

The temperature efficiency of the baseline aluminum heat wheel without considering the LHC effect ($\lambda = 0$), represented by the red dashed line, increases almost linearly when decreasing the airflow rate. The trend can be justified by the increased NTU in Eq. (1) owing to the reduced airflow rates. The term on the right in the parenthesis in Eq. (1) has minimal influence on temperature efficiency at a rotation speed of 10 RPM. The efficiency values are above 85 % within the full range of airflow rates from 150 m^3/h to 500 m^3/h. In contrast, the temperature efficiency, which is represented by a blue line in Fig. 3 (A), taking the LHC effect into account, exhibits the opposite trend when airflow rates decrease. The decreasing airflow rates lead to the increased heat transfer ability of the heat wheel represented by the increased NTU in Fig. 3 (B). Moreover, the decreasing airflow rates aggravate the longitudinal heat conduction effect, which counteracts the effect of the increased NTU on the temperature efficiency. In relatively low airflow rates (150 m^3/h to 300 m^3/h), the increased longitudinal heat conduction effect prevails as indicated in Fig. 3 (C)and the temperature efficiency drops by reducing the airflow rate. From 300 m^3/h to 500 m^3/h, the effects of the variations of the NTU and the longitudinal heat conduction compensate each other. The temperature efficiency is relatively constant over this airflow range. The efficiency drop when considering LHC represented by the shaded region lowers from 18 % to 6 % with increasing ventilation rates as shown in the filled region in Fig. 3 (A). The temperature efficiency with the LHC effects is under 85 % for the typical single family house ventilation rates. It can be confirmed from

Fig. 3 that the LHC effect significantly degrades the temperature efficiency in a heat wheel made of a highly conductive material. The finding from Fig. 3 also suggests that, contrary to early experience, increasing NTU by enlarging heat transfer area may worsen the temperature efficiency resulting from the LHC effect. If the LHC effect is neglected, the intended high efficiency design is often not achieved in practice. One can conclude that the highly efficient heat recovery (>85%) may not be achieved with a common aluminum heat wheel. It is incorrect to extrapolate temperature efficiency using testing efficiency values under high airflow rates or to scale down big heat wheels with the $\varepsilon - NTU$ approach if the effect of LHC is neglected. In contrast to the expectation of the typical engineering design, enlarging the heat wheel may deteriorate the temperature efficiency instead of improving the performance.

3.2. Parametric analysis

Parametric analysis is performed to assess the influence of individual design and operating parameters on NTU, the LHC effect and resulting temperate efficiency. The potential influencing design parameters for improving heat wheel recovery efficiency are identified through parametric analysis.

The studied aluminum heat wheel in section 3.1 is used as a reference case in parametric analysis, which is denoted by 0 % change for the parameter in Fig. 4. The studied parameters are variations of ±5%, ±15%, ±25%, ±50%, and ±75% of the initial values of airflow rates, wheel diameter and depth, wall thermal conductivity and thickness, and the rotary speed of the wheel. Only one parameter is changed at one time, and the remaining parameters remain at the reference value. The results of the changed per cent of efficiency for NTU and λ corresponding with changed parameters are displayed in Fig. 4. The changes in NTU and λ in Fig. 4 (B) and (C) can be justified by Eqs. (6) and (7). Fig. 4 (A) shows that the temperature efficiency is relatively sensitive to wheel diameter and wheel depth, airflow rate, wall thickness and thermal conductivity. Reducing wheel diameter can reduce both λ and NTU, but the resulting efficiency is, however, lower than the reference value. The sharply reduced efficiency, when reducing the wheel diameter by 75%, indicates that the reduction of NTU dominates for small wheels despite the LHC effect being simultaneously reduced. A wheel design with a minimal wheel diameter should therefore be avoided.

As shown by the points in the yellow highlighted region in Fig. 4 (A), the most influencing parameters for improving the temperature efficiency are matrix thickness and thermal conductivity of the matrix and wheel depth. Reducing matrix thickness, thermal conductivity and increasing wheel depth result in higher temperature efficiency as the LHC is lowered, as justified by Eq. (6). A deeper wheel, however, means a higher pressure drop through the heat wheel. Additionally, the deep wheel may cause high noise levels, which is a significant concern in the application of residential buildings. Lower conductive materials and thin walls may be used to increase the temperature efficiency because they diminish the LHC effect and keep the NTU unchanged without introducing an additional pressure drop penalty.

The temperature efficiency for the heat wheels with different matrix materials (aluminum, stainless steel and carbonate plastic) and different channel shapes (sinusoidal, circular, rectangular) are computed according to Eqs. (1)-(10) and shown in Fig. 5. All the dashed lines represent the temperature efficiency excluding LHC ($\lambda = 0$). The solid lines denote temperature efficiencies including the LHC. The difference between the two lines, which is defined as the efficiency loss resulting from the LHC effect for different materials and channel shapes. The calculated temperature efficiency excluding the LHC effect for most of the studied wheels is rather high. However, efficiency loss is caused when the LHC is considered. The efficiency loss owing to the presence of LHC for the aluminum wheel (represented by the slash lines in Fig. 5) is the most significant. The efficiency loss for stainless steel wheels due to LHC (represented by the red shaded area in Fig. 5) is insignificant. For plastic wheels, there is no LHC for all the three channel shapes due to their low thermal conductivity. Therefore, the temperature efficiency of plastic wheels is identical for the cases including and excluding the LHC effect. The circular plastic heat wheel provides the highest temperature efficiency compared to the other two shapes. The circular channel has no sharp corner, thus, the peripheral temperature gradients are minimum for all the materials. As an example, the Nusselt number is a constant of 4.36 for the circular plastic channel. As a comparison, the Nusselt number are about 1.5 and 3.0 for the wheel with sinusoidal and rectangular plastic channels, respectively. Hence, the temperature efficiency of the plastic wheel with a circular channel shape is higher relative to the wheel with sinusoidal and rectangular shapes resulting from the higher convective heat transfer coefficients. The efficiency dramatically drops with increasing airflow rates for the wheels with sinusoidal and rectangular channel shapes. Sinusoidal and rectangular channel shapes introduce sharp corners where the temperature gradients exist in the peripheral direction for poorly conductive plastic. Stainless steel wheels with sinusoidal and circular channels can provide high efficiency. However, the high cost

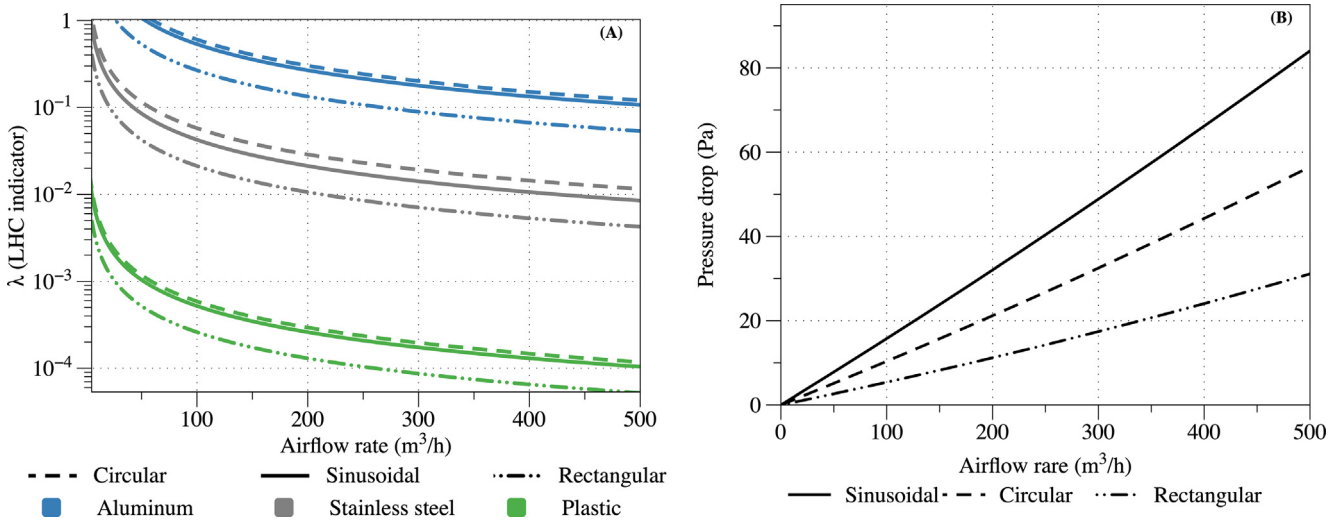

Fig. 6. (A) LHC indicator λ and (B) pressure drop vs airflow rate with different channel shapes.

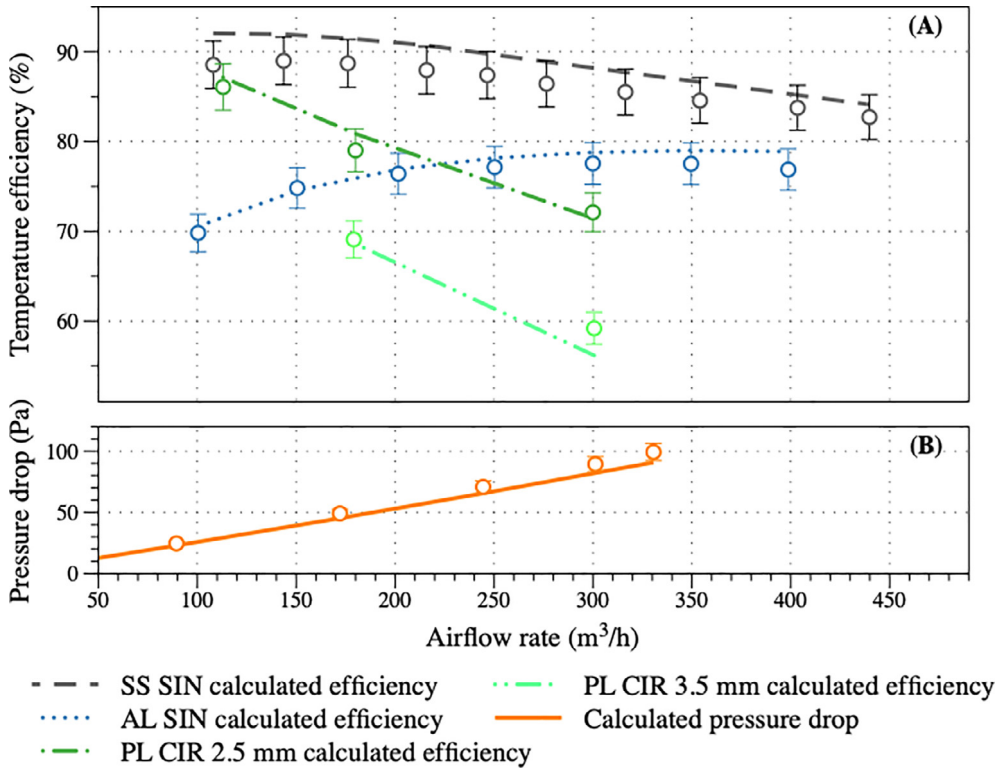

Fig. 7. Experimental verification for (A) temperature efficiency and (B) pressure drop for the developed heat wheels.

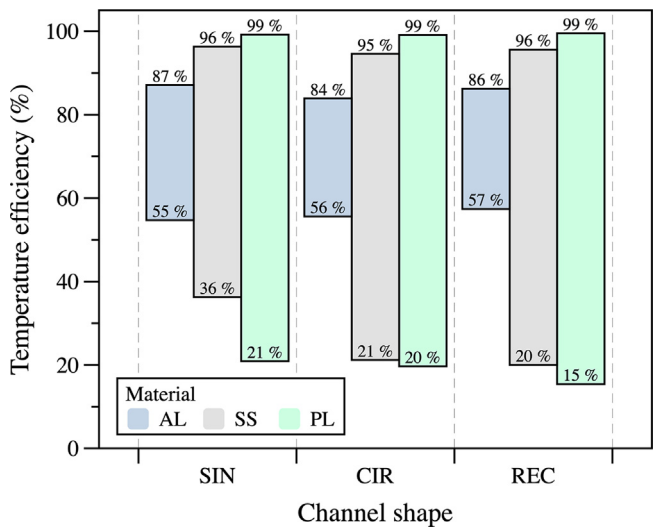

Fig. 8. Highest and lowest temperature efficiency for aluminum, stainless steel and carbonate plastic wheels with sinusoidal, circular and rectangular channel shapes at an airflow rate of 200 m^3/h.

of stainless steel, as well as its stiffness and heavy wheel due to its high density, may hinder its application. Carbonate plastic heat wheels can provide high efficiency (>90%) at low airflow rates, e.g. from 150 m^3/h to 300 m^3/h.

Fig. 6 shows λ (the LHC indicator) and the pressure drop for different channel shapes and materials. The pressure drop is sensitive to channel shapes but not the matrix material due to the laminar nature of the airflow. It can be found from Fig. 6 that the carbonate plastic heat wheel with a circular channel shape can provide an extremely low LHC and a relatively low pressure drop. Thus, the plastic heat wheel with circular channels is a promising solution to provide high efficiency at a low pressure drop through the wheel. It can be seen from Fig. 6 that there is a steep drop in the value of the LHC indicator λ with increasing airflow rates, which is determined according to Eq. (6). Compared to stainless steel and plastic wheels, aluminum wheels have an LHC indicator λ that is one and three orders of magnitude higher respectively. This trend confirms that the LHC plays a big role in degrading temperature efficiency for aluminum heat wheels at low airflow rates.

3.3. Verification with developed aluminum, stainless steel and plastic heat wheels

Four heat wheels with different materials and corrugation shapes were constructed and tested to validate the theoretical development of the highly efficient heat wheels. The specifications of the four heat wheels are given in Section 2.3. The construction of these four heat wheels was limited by the available materials in this study. For instance, the circular channel with a diameter smaller than 2.5 mm for plastic wheel was not obtained in this study despite the fact that a smaller diameter can yield higher efficiency. Another example is that the rectangular channel was not available for the wheels with these three materials (aluminum, stainless steel and plastic). However, the contracted heat wheels, which cover three different materials and two different corrugations, provide adequate validation for the theoretical development of highly efficient heat wheels. The measurement uncertainties for temperature efficiency and pressure drop are assessed with the method addressed in Section 2.3. As shown in Fig. 7, the predicted values for efficiency and pressure drop are in good agreement with experimental results. The constructed stain steel heat wheel (SS SIN) with a sinusoidal channel shape can provide the highest temperature efficiency at all airflow rates. The plastic heat wheel with circular channel shape (PL CIR 2.5 mm) offers relatively high efficiency at low airflow rates. However, the efficiency drops dramatically since the decrease of NTU prevails with the increasing

airflow rates. The temperature efficiency of aluminum heat wheel with sinusoidal channel shape (AL SIN) at low airflow rates is lower than its efficiency at high airflow rates due to the dominant LHC effect at low rates as aforesaid. Based on these findings, different heat wheels aiming to achieve high efficiency can be designed and selected according to their operating airflow rates.

This study focuses on the development of highly efficient heat wheels for cold climates. The rotary heat exchangers developed can be extended in their applications for cooling working conditions where heat recovery with high efficiency is required when no phase change of air occurs inside the heat wheel. Since heat wheels operate under no-phase-change conditions, the temperature efficiency and pressure drop should not be affected by operating temperatures or humidity.

3.4. Optimization of the heat wheel by studying the best and worst practice of the heat wheel designs for temperature efficiency

The highest and lowest temperature efficiency, given design input ranges and values of the parameters in Table 3, are found with the pattern search optimization addressed in Section 2.4. These represent the best and worst heat wheel designs with respect to operational temperature efficiency and are shown in Fig. 8. At a nominal ventilation rate of 200 m^3/h, highly efficient heat wheels (with efficiency > 85 %) can be realized with the optimal design for all cases except for the aluminum wheel with a circular channel shape. The plastic and stainless steel wheels present reasonably high efficiency (>95%). However, the pressure drop for these optimized heat wheels should also be taken into account. In addition, these high temperature efficiencies may lead to more condensation and frosting risk in heat wheels in winter in cold regions and more overheating risk in shoulder seasons. Proper efficiency regulations and controls thus need to be further developed for these highly efficient heat wheels. Nevertheless, the corresponding development of regulations and controls is beyond the scope of this study. The temperature efficiency of plastic and stainless steel wheels ranges is wider compared to the aluminum wheels. One can conclude that highly efficient heat recovery is achievable when the optimal design is applied. The efficiency of the plastic and stainless steel heat wheels is more sensitive to the design parameters than aluminum wheels. In addition, wheels should be specifically sized based on these parameters, particularly when designing plastic heat wheels, where bad designs can result in temperatures as low as 15%-20%.

4. Conclusions

As a means of achieving highly energy-efficient ventilation in zero-emission buildings, heat wheels with high temperature efficiency, which is superior to today's solutions, are needed. In this regard, the performance of heat wheels has been theoretically and experimentally studied and assessed for different corrugations and materials. The LHC has been identified as the essential factor limiting the maximum temperature efficiency for the widely used aluminum heat wheel. This study's finding suggests that the heat wheels' temperature efficiency may be greatly overestimated if the LHC effect is ignored, especially for highly conductive materials like aluminum. Contrary to the earlier experience, the design of big heat wheels with the intention of achieving high temperature efficiency may actually deteriorate efficiency since LHC can be higher in these big heat wheels. According to the parametric study, reducing matrix wall thickness for highly conductive materials and low conductive materials can significantly improve temperature efficiency. The stainless steel and plastic heat wheels can exhibit high temperature efficiency above 90 %. However, the high cost and stiffness of stainless steel may restrict its use in heat wheels. Plastic wheels with circular channels that are symmetrical could provide a promising solution to meet the high temperature efficiency need in the future. Based on the optimization of the studied heat wheels, it has been demonstrated that a high heat recovery efficiency (>85 %) can be achieved for the commonly used aluminum heat wheels if the optimum design is applied in practice. Developed heat wheels with a high temperature efficiency may lead to more condensation and frosting risk in winter as well as higher overheating risk during shoulder seasons. In order to adapt heat wheels with high efficiency, their controls need be modified or developed further. Furthermore, it shows that plastic heat wheels are relatively sensitive to the design parameters relative to the aluminum and stainless steel wheels. This study develops highly efficient rotary heat wheels for cold climates, however, the applications can be extended to warm operating conditions when no phase change in air occurs.

Declaration of Competing Interest

The authors declare that they have no known competing financial interests or personal relationships that could have appeared to influence the work reported in this paper.

Acknowledgement

This research was funded by the Research Council of Norway (NFR) and Flexit AS through the EnergiBolig project (NFR grant number: 256474). The authors would like to acknowledge Lars Wessman and the laboratory in Flexit for the experimental tests that significantly improved this work.

References

[1] P. Ekins, E. Lees, The impact of EU policies on energy use in and the evolution of the UK built environment, Energy Policy 36 (12) (Dec. 2008) 4580–4583.
[2] X. Kong, S. Lu, Y. Wu, A review of building energy efficiency in China during 'Eleventh Five-Year Plan' period, Energy Policy 41 (2012) 624–635.
[3] T.A. Nguyen, M. Aiello, Energy intelligent buildings based on user activity: A survey, Energy Build. 56 (2013) 244–257.
[4] N. Hamza, R. Gilroy, The challenge to UK energy policy: An ageing population perspective on energy saving measures and consumption, Energy Policy 39 (2) (2011) 782–789.
[5] L. Pérez-Lombard, J. Ortiz, C. Pout, A review on buildings energy consumption information, Energy Build. 40 (3) (2008) 394–398.
[6] IEA, Renewable for heating and cooling: untapped potential, OECD/IEA (2007).
[7] M. Fehrm, W. Reiners, M. Ungemach, Exhaust air heat recovery in buildings, Int. J. Refrig. 25 (4) (2002) 439–449.
[8] P. Liu, H.M. Mathisen, M. Justo Alonso, C. Simonson, A frosting limit model of air-to-air quasi-counter-flow membrane energy exchanger for use in cold climates, Appl. Therm. Eng. 111 (2017).
[9] P. Liu, M. Justo Alonso, H.M. Mathisen, C. Simonson, Energy transfer and energy saving potentials of air-to-air membrane energy exchanger for ventilation in cold climates, Energy Build. 135 (2017) 95–108.
[10] M. Justo Alonso, P. Liu, H.M. Mathisen, G. Ge, C. Simonson, Review of heat/energy recovery exchangers for use in ZEBs in cold climate countries, Build. Environ. 84 (2015) 228–237.
[11] H.Y. Bai, P. Liu, M. Justo Alonso, H.M. Mathisen, A review of heat recovery technologies and their frost control for residential building ventilation in cold climate regions, Renewable and Sustainable Energy Reviews 162 (2022).
[12] "Byggteknisk forskrift (TEK17) - Direktoratet for byggkvalitet." [Online]. Available: https://dibk.no/byggereglene/byggteknisk-forskrift-tek17/. [Accessed: 05-Dec-2018].
[13] C.J. Simonson, R.W. Besant, Heat and Moisture Transfer in Energy Wheels During Sorption, Condensation, and Frosting Conditions, J. Heat Transfer 120 (3) (Aug. 1998) 699.
[14] D.W. Ruth, D.R. Fisher, H.N. Gawley, Investigation of frosting in rotary air-to-air heat exchangers, ASHRAE Trans. 81 (1975) 410–417.
[15] P. Liu, M. Justo Alonso, H. M. Mathisen, and A. Halfvardsson, The use of machine learning to determine moisture recovery in a heat wheel and its impact on indoor moisture, *Build. Environ.*, vol. 215, p. 108971, May 2022.
[16] R.K. Shah, D.P. Sekulic, Fundamentals of Heat Exchanger Design, John Wiley & Sons, 2003.
[17] P. Liu, H.M. Mathisen, M.J. Alonso, Theoretical Prediction of Longitudinal Heat Conduction Effects on the Efficiency of the Heat Wheel used for Ventilation in Powerhouse Building 'kjørbo' in Norway, Energy Procedia 105 (2017) 4949–4954.

[18] C. A. Roulet, F. . Heidt, F. Foradini, and M.-C. Pibiri, "Real heat recovery with air handling units," *Energy Build.*, vol. 33, no. 5, pp. 495–502, May 2001.
[19] C.A. Roulet, Ventilation and airflow in buildings : methods for diagnosis and evaluation, Earthscan, 2008.
[20] Ø. Rønneseth, P. Liu, M.J. Alonso, Airflow Measurements for Air Handling Units, SINTEF Report (2018).
[21] S. Bilodeau, P. Brousseau, M. Lacroix, Y. Mercadier, Frost formation in rotary heat and moisture exchangers, Int. J. Heat Mass Transf. 42 (14) (Jul. 1999) 2605–2619.
[22] M. Rafati Nasr, M. Fauchoux, R.W. Besant, C.J. Simonson, A review of frosting in air-to-air energy exchangers, Renew. Sustain. Energy Rev., Feb. 30 (2014) 538–554.
[23] G.D. Bahnke, C.P. Howard, The Effect of Longitudinal Heat Conduction on Periodic-Flow Heat Exchanger Performance, J. Eng. Power 86 (2) (Apr. 1964) 105.
[24] R.K. Shah, A Correlation for Longitudinal Heat Conduction Effects in Periodic-Flow Heat Exchangers, J. Eng. Power 97 (3) (Jul. 1975) 453.
[25] T. Skiepko, The effect of matrix longitudinal heat conduction on the temperature fields in the rotary heat exchanger, Int. J. Heat Mass Transf. 31 (11) (Nov. 1988) 2227–2238.
[26] R. K. Ramesh K. . Shah and A. L. Alexander L. London, Laminar flow forced convection in ducts : a source book for compact heat exchanger analytical data, p. 477, 1978.
[27] K.M. Smith, S. Svendsen, Development of a plastic rotary heat exchanger for room-based ventilation in existing apartments, Energy Build. 107 (2015) 1–10.
[28] V.Y. Borodulin, M.I. Nizovtsev, A criterial analysis of the effectiveness of air-to-air heat exchangers with periodic change of airflow direction, Appl. Therm. Eng. 130 (Feb. 2018) 1246–1255.
[29] H.J. Chung, J.S. Lee, C. Baek, H. Kang, Y. Kim, Numerical analysis of the performance characteristics and optimal design of a plastic rotary regenerator considering leakage and adsorption, Appl. Therm. Eng. 109 (2016) 227–237.
[30] W.M. Kays, A.L. London, *Compact Heat Exchangers*. Krieger Publishing Company (1984).
[31] EN 308:1997 - Heat exchangers. Test procedures for establishing the performance of air to air and flue gases heat recovery devices.
[32] ISO 5167-1, "Measurement of fluid flow by means of pressure differential devices - Part 1: Orifice plates, nozzles and Venturi tubes inserted in circular cross-section conduits running full," International Standards Organization, Geneva, Switzerland., 2003.
[33] ISO 5167-2:2003 - Measurement of fluid flow by means of pressure differential devices inserted in circular cross-section conduits running full – Part 2: Orifice plates.
[34] H. W. Coleman and W. G. Steele, "Experimentation, Validation, and Uncertainty Analysis for Engineers: Third Edition," *Exp. Validation, Uncertain. Anal. Eng. Third Ed.*, pp. 1–317, Jul. 2009.
[35] V. Torczon, "On the Convergence of Pattern Search Algorithms," *http://dx.doi.org/10.1137/S1052623493250780*, vol. 7, no. 1, pp. 1–25, Jul. 2006.